A priory study of velocity-pressure-gradient and pressure-dilatation terms in transport equations for subfilter turbulent kinetic energy

A PRIORY STUDY OF VELOCITY-PRESSURE-GRADIENT AND PRESSURE-DILATATION TERMS IN TRANSPORT EQUATIONS FOR SUBFILTER TURBULENT KINETIC ENERGY

A.N. Lipatnikov* and V.A. Sabelnikov**
lipatn@chalmers.se
*Chalmers University of Technology, Gothenburg, 412 96, Sweden
**ONERA - The French Aerospace Lab., F-91761 Palaiseau, France

Abstract

In the paper, pressure-dilatation and velocity-pressure-gradient terms in transport equations for subfilter turbulent kinetic energy are *a priori* explored by analyzing three-dimensional Direct Numerical Simulation (DNS) data obtained earlier from a moderately lean (the equivalence ratio $\Phi = 0.81$) complex-chemistry hydrogen-air flame propagating in a box. The DNS conditions are associated with moderately intense (Kolmogorov time scale is shorter than flame time scale by a factor of above two), small-scale (Kolmogorov length scale is smaller than thermal laminar flame thickness by a factor of about 20) turbulence. The studied terms are computed by filtering out the DNS fields of velocity, density, pressure, and fuel mass fraction and adopting Gaussian or top hat filters of different widths, which are smaller or comparable with laminar flame thickness. Moreover, gradient models of the second order generalized central moments (joint cumulants), which are mainly applied to subfiter turbulent stresses and scalar fluxes in various flows, are extended to close the explored pressure-containing terms. Obtained results give priority to using the velocity-pressure-gradient term when compared to the pressure-dilatation term. Specifically, first, the former term is weakly sensitive to filter shape, whereas the latter term evaluated adopting the Gaussian filter is significantly larger than the same term yielded by the top-hat filter of the same width. Second, spatial variations of time- and transverse averaged velocity-pressure-gradient term within mean flame brush are well predicted by the newly introduced gradient model in all studied cases. While the sole model constant tuned to get the best prediction increases gradually with filter width, the constant remains of unity order in all cases. These results encourage further assessment of gradient models as a promising tool for large eddy simulation of premixed turbulent combustion.

Introduction

Since pioneering studies by Karlovitz et al. [1] and by Scurlock and Grover [2] the influence of combustion-induced thermal expansion on turbulence was addressed in numerous papers reviewed elsewhere [3-6]. The most common approach to allowing for such effects in numerical simulations of premixed combustion consists in using a transport equation for turbulent kinetic energy, which can be written in different forms, e.g.,

$$\frac{\partial}{\partial t}\left(\bar{\rho}\tilde{k}\right) + \frac{\partial}{\partial x_i}\left(\bar{\rho}\tilde{u}_i\tilde{k}\right) + \frac{\partial}{\partial x_i}\left[\bar{\rho}\left(\frac{\widetilde{u_i u_j^2}}{2} - \frac{\tilde{u}_i\widetilde{u_j^2}}{2} - \tilde{u}_j\widetilde{u_i u_j} + \tilde{u}_i\tilde{u}_j^2\right) - \overline{u_j\tau_{\mu,ij}} + \bar{u}_j\bar{\tau}_{\mu,ij} + \overline{pu_i} - \bar{p}\bar{u}_i\right]$$
$$= -\bar{\rho}\tilde{\tau}_{ij}\frac{\partial\tilde{u}_j}{\partial x_i} + \left(\tilde{u}_i - \bar{u}_i\right)\frac{\partial\bar{p}}{\partial x_i} + \overline{p\frac{\partial u_i}{\partial x_i}} - \bar{p}\frac{\partial\bar{u}_i}{\partial x_i} - \left(\tilde{u}_j - \bar{u}_j\right)\frac{\partial\bar{\tau}_{\mu,ij}}{\partial x_i} - \overline{\tau_{\mu,ij}\frac{\partial u_j}{\partial x_i}} + \bar{\tau}_{\mu,ij}\frac{\partial\bar{u}_j}{\partial x_i} \quad (1)$$

or

$$\frac{\partial}{\partial t}\left(\bar{\rho}\tilde{k}\right)+\frac{\partial}{\partial x_i}\left(\bar{\rho}\tilde{u}_i\tilde{k}\right)+\frac{\partial}{\partial x_i}\left[\bar{\rho}\left(\frac{\widetilde{u_i u_j^2}}{2}-\frac{\tilde{u}_i\widetilde{u_j^2}}{2}-\tilde{u}_j\widetilde{u_i u_j}+\tilde{u}_i\tilde{u}_j^2\right)\right]$$
$$=-\bar{\rho}\tilde{\tau}_{ij}\frac{\partial\tilde{u}_j}{\partial x_i}+\left(\tilde{u}_i-\bar{u}_i\right)\frac{\partial\bar{p}}{\partial x_i}-\overline{u_i\frac{\partial p}{\partial x_i}}+\bar{u}_i\frac{\partial\bar{p}}{\partial x_i}-\left(\tilde{u}_j-\bar{u}_j\right)\frac{\partial\bar{\tau}_{\mu,ij}}{\partial x_i}+\overline{u_j\frac{\partial\tau_{\mu,ij}}{\partial x_i}}-\bar{u}_j\frac{\partial\bar{\tau}_{\mu,ij}}{\partial x_i}. \tag{2}$$

Here, for an arbitrary quantity, $\bar{q}$ designates either its ensemble-averaged value within Reynolds-Averaged Navier-Stokes (RANS) framework or its spatially filtered value within Large Eddy Simulation (LES) framework; $\tilde{q}=\overline{\rho q}/\bar{\rho}$ refers to Favre-averaged or Favre-filtered quantity; t and x_i are time and Cartesian coordinates, respectively; $\tilde{k}=0.5\left(\widetilde{u_i u_i}-\tilde{u}_j^2\right)$ and $\tilde{\tau}_{ij}=\widetilde{u_i u_j}-\tilde{u}_i\tilde{u}_j$ are turbulent kinetic energy and Reynolds stress tensor, respectively, within RANS framework or subfilter-scale kinetic energy and stress tensor, respectively, within LES framework; ρ and p are density and pressure, respectively; u_i are components of the velocity vector $\mathbf{u}$; $\tau_{\mu,ij}$ is viscous stress tensor, with μ referring to dynamic viscosity; and the summation convention applies to repeated indexes. The sole difference between Eqs. (1) and (2) consists of either splitting terms that involve the stress tensor $\sigma_{ij}=\tau_{\mu,ij}-p\delta_{ij}$ into a transport term and a source/sink term, i.e., $\partial\left(u_j\sigma_{ij}\right)/\partial x_i$ and $\sigma_{ij}\,\partial u_j/\partial x_i$ in the left and right hand sides of Eq. (1), respectively (lhs and rhs, respectively), or using the single term $u_j\,\partial\sigma_{ij}/\partial x_i$ on the rhs of Eq. (2). Here, δ_{ij} is Kronecker delta. In combustion literature the former and latter approaches were used, e.g., in Refs. [6-8] and [8-12], respectively.

Since

$$\frac{\partial}{\partial x_i}\left(-\overline{u_j\sigma_{ij}}+\bar{u}_j\bar{\sigma}_{ij}\right)=-\overline{\sigma_{ij}\frac{\partial u_j}{\partial x_i}}+\bar{\sigma}_{ij}\frac{\partial\bar{u}_j}{\partial x_i}-\overline{u_j\frac{\partial\sigma_{ij}}{\partial x_i}}+\bar{u}_j\frac{\partial\bar{\sigma}_{ij}}{\partial x_i}, \tag{3}$$

Eqs. (1) and (2) are mathematically identical. However, differences between the stress terms written in these two different forms could be significant in numerical simulations of turbulent combustion. The point is that contrary to low-Mach-number flows without heat release, where both local and mean dilatations are very small, magnitudes of terms $\overline{p\Theta}$ and $\bar{p}\bar{\Theta}$ can be much larger than magnitudes of other terms in Eq. (1) in flames where significant (i.e., comparable with other velocity derivatives even after averaging) dilatation $\Theta=\nabla\cdot\mathbf{u}$ is multiplied with a very large pressure $O(10^5)$ N/m^2. Therefore, variations in the difference in $\overline{p\Theta}$ and $\bar{p}\bar{\Theta}$ on the rhs of Eq. (1), e.g., due to the use of different filters within LES framework, can be significant when compared to other terms in Eq. (1). On the contrary, such a problem does not arise for the substantially smaller terms $\overline{\mathbf{u}\cdot\nabla p}$ and $\bar{\mathbf{u}}\cdot\nabla\bar{p}$.

Accordingly, one goal of the present work is to perform *a priori* comparison of utility of the two discussed forms of presentation of the filtered pressure terms in Eqs. (1) and (2) for LES of premixed turbulent combustion. For these purposes, Direct Numerical Simulation (DNS) data created by Dave et al. [13,14] are analyzed. Another goal of the study consists in assessing gradient models of these pressure terms by processing the same DNS data.

Such gradient models are introduced in the next section. In the third section, the DNS attributes are briefly reported, followed by presentation and discussion of computed results in the fourth section. Conclusions are drawn in the fifth section.

Gradient Models

Gradient models of the second order generalized central moments (joint cumulants) [15,16] of two fields $f(\mathbf{x},t)$ and $g(\mathbf{x},t)$, i.e.,

$$\bar{\tau}(f,g)\equiv\overline{fg}-\bar{f}\bar{g} \qquad \text{or} \qquad \tilde{\tau}(f,g)\equiv\widetilde{fg}-\tilde{f}\tilde{g}, \tag{4}$$

were pioneered by Leonard [17] and by Clark et al. [18]. In LES studies of premixed turbulent flames, such models were successfully applied to $\tilde{\tau}(u_i, u_j)$, $\tilde{\tau}(u_i, c)$, and $\tilde{\tau}(c, c)$ [6,19-23]. To the best of our knowledge, gradient models have not yet been applied to $\bar{\tau}(p, \Theta)$ or $\bar{\tau}(u_i, \partial p/\partial x_i)$, at least in combustion literature,

Following Refs. [24-26], let's derive gradient model equations by (i) applying Taylor expansion to a similarity model by Bardina et al. [27], which was proposed for incompressible flows, and (ii) considering the lowest-order terms.

The similarity model reads

$$\bar{\tau}(f, g) \approx \bar{\tau}(\bar{f}, \bar{g}) = \overline{\bar{f}\bar{g}} - \bar{\bar{f}}\bar{\bar{g}}. \tag{5}$$

As shown by Cimarelli et al. [25], Eq. (5) can be rewritten in the following form

$$\bar{\tau}(f, g) \approx \frac{1}{2} \iint G(\mathbf{x}, \boldsymbol{\eta}) G(\mathbf{x}, \boldsymbol{\xi}) \left[\bar{f}(\boldsymbol{\xi}, t) - \bar{f}(\boldsymbol{\eta}, t)\right] [\bar{g}(\boldsymbol{\xi}, t) - \bar{g}(\boldsymbol{\eta}, t)] d^3\boldsymbol{\xi} d^3\boldsymbol{\eta} \tag{6}$$

using Eq. (1) and the following identities:

$$\iint G(\mathbf{x}, \boldsymbol{\eta}) G(\mathbf{x}, \boldsymbol{\xi}) \bar{f}(\boldsymbol{\xi}, t) \bar{g}(\boldsymbol{\eta}, t) d^3\boldsymbol{\xi} d^3\boldsymbol{\eta} = \bar{\bar{f}}\bar{\bar{g}}, \tag{7}$$

$$\iint G(\mathbf{x}, \boldsymbol{\eta}) G(\mathbf{x}, \boldsymbol{\xi}) \bar{f}(\boldsymbol{\xi}, t) \bar{g}(\boldsymbol{\xi}, t) d^3\boldsymbol{\xi} d^3\boldsymbol{\eta} = \overline{\bar{f}\bar{g}}. \tag{8}$$

Here, $G(\mathbf{x}, \boldsymbol{\xi})$ is a generic filter kernel in space and

$$\int G(\mathbf{x}, \boldsymbol{\xi}) d^3\boldsymbol{\xi} = 1. \tag{9}$$

Application of the first-order Taylor expansion to the differences inside the integral in Eq. (6) results in

$$\bar{\tau}(f, g) \approx \frac{\partial \bar{f}}{\partial x_j} \frac{\partial \bar{g}}{\partial x_k} \frac{1}{2} \iint G(\mathbf{x}, \boldsymbol{\eta}) G(\mathbf{x}, \boldsymbol{\xi}) (\xi_j - \eta_j)(\xi_k - \eta_k) d\boldsymbol{\xi} d\boldsymbol{\eta} = \tau(x_j, x_k) \frac{\partial \bar{f}}{\partial x_j} \frac{\partial \bar{g}}{\partial x_k} \tag{10}$$

or

$$\bar{\tau}(f, g) \approx \frac{1}{12} \Delta^2 \frac{\partial \bar{f}}{\partial x_k} \frac{\partial \bar{g}}{\partial x_k} \tag{11}$$

for a regular Cartesian control volume and a top-hat filter of width Δ, i.e.,

$$G_\Delta(\mathbf{x}, \boldsymbol{\xi}) = \frac{1}{\Delta^3} \left[1 - \mathrm{H}\left(|\boldsymbol{\xi}| - \frac{\Delta}{2}\right)\right], \tag{12}$$

where H is Heaviside function. Equation (11) constitutes the gradient model for the fields f and g. Specifically, Eq. (11) reads

$$\bar{\tau}(p, \Theta) = \overline{p\Theta} - \bar{p}\bar{\Theta} = \frac{1}{12} \Delta^2 \frac{\partial \bar{p}}{\partial x_k} \frac{\partial \bar{\Theta}}{\partial x_k} \tag{13}$$

and

$$\bar{\tau}(\mathbf{u}, \nabla p) = \overline{u_i \frac{\partial p}{\partial x_i}} - \bar{u}_i \overline{\frac{\partial p}{\partial x_i}} = \frac{1}{12} \Delta^2 \frac{\partial \bar{u}_i}{\partial x_k} \frac{\partial^2 \bar{p}}{\partial x_i \partial x_k}. \tag{14}$$

Equations (13) and (14) are assessed in the rest of the paper.

DNS Attributes and Diagnostic Methods

Since DNS database was discussed by Dave et al. [13,14] and by the present authors in previous articles [28-35], only a summary of the DNS attributes is given below. The reader interested in further details is referred to the cited papers.

A statistically planar and one-dimensional, lean H_2-air turbulent flame propagating in a cuboid (19.18 × 4.8 × 4.8 mm) was simulated by adopting the Pencil code [36] to numerically solve unsteady and three-dimensional continuity, compressible Navier-Stokes, species and energy transport equations supplemented with the mixture-averaged molecular transfer model and a detailed chemical mechanism (9 species and 21 reactions) by Li et al. [37]. The cuboid was meshed with a uniform grid of $960 \times 240 \times 240$ cells. At the transverse sides, boundary conditions were periodic. At the inlet and outlet, Navier-Stokes Characteristic Boundary Conditions (NSCBC) [38] were set.

To pre-generate homogeneous isotropic turbulence in another cube with the fully periodic boundary conditions, large-scale forcing was adopted [13]. The turbulence was allowed to evolve until a statistically stationary state was reached. At this final stage, the rms velocity $u' =$ 6.7 m/s; an integral length scale $L = 3.1$ mm; the integral time scale $\tau_t = L/u' = 0.46$ ms; the turbulent Reynolds number $Re_t = u'L/\nu = 950$; the Kolmogorov time scale $\tau_\eta = (\nu/\langle\varepsilon\rangle)^{1/2} = 0.015$ ms; and the Kolmogorov length scale $\eta = (\nu^3/\langle\varepsilon\rangle)^{1/4} = 0.018$ mm. Here, ν is kinematic viscosity; $\langle\varepsilon\rangle = \langle 2\nu S_{ij}S_{ij}\rangle$ is the turbulence dissipation rate averaged over the cube; and $S_{ij} = \left(\partial u_i/\partial x_j + \partial u_j/\partial x_i\right)/2$ is the rate-of-strain tensor.

At $t = 0$, a pre-computed planar laminar flame (the equivalence ratio $\Phi = 0.81$, the pressure $P = 1$ bar, and the unburned gas temperature T_u =310 K) was embedded into the cuboid at $x = x_0$. The laminar flame speed S_L, thickness $\delta_L = \max\{|\nabla T|\}/(T_b - T_u)$, and time scale $\tau_f = \delta_L/S_L$ are equal to 1.84 m/s, 0.36 mm, and 0.20 ms, respectively. Here, subscripts u and b refer to unburned and burned mixtures, respectively. Subsequently, the flame was wrinkled and stretched by the pre-generated turbulence, which was continuously injected into the computational domain through its left boundary $x = 0$ and decayed along the x-direction. It is worth stressing that for the equivalence ratio $\Phi = 0.81$ addressed in the present work, diffusional-thermal effects discussed in detail elsewhere [39-41] are weakly pronounced despite the mixture is lean. For instance, a ratio of turbulent burning velocity to flame surface area is close to S_L [31, Fig. 3].

The Karlovitz number $Ka = \tau_f/\tau_\eta$ and the Damköhler number $Da = LS_L/(u'\delta_L)$, evaluated using characteristics of the pre-generated turbulence, are equal to 13 and 2.35, respectively. Due to decay of the injected statistically stationary turbulence with distance x from the inlet, the turbulence characteristics averaged over the cuboid cross-section nearest to a plane where the transverse-averaged $\langle c\rangle(x,t) = 0.01$ (leading edge of the mean flame brush) are different: $u' = 3.3$ m/s; the Taylor length scale $\lambda = \left(10\nu_u\overline{\langle k\rangle}/\overline{\langle\varepsilon\rangle}\right)^{1/2} = 0.25$ mm or $0.69\delta_L^T$; $\eta = 0.018$ mm or $0.05\delta_L^T$; $\tau_\eta = 0.087$ ms; $Re_\lambda = u'\lambda/\nu_u = 55$; and $Ka = 2.3$ is much less than $(\delta_L/\eta)^2 \cong 400$, because $S_L\delta_L/\nu_u \gg 1$ in moderately lean hydrogen-air mixtures [42]. Here, $c = 1 - Y_F/Y_{F,u}$ is the fuel-based combustion progress variable; Y_F is fuel mass fraction; $\overline{\langle k\rangle}$ and $\overline{\langle\varepsilon\rangle}$ are time- and transverse-averaged turbulent kinetic energy and its dissipation rate, respectively, sampled at 58 instants from 1.0 to 1.57 ms. Henceforth, $\overline{\langle\cdot\rangle}$ designates time- (overline) and transverse-averaged (angles) value of a local or filtered quantity, e.g., $\overline{\langle\bar{p}\rangle}(x)$ refers to axial variations of the filtered pressure field $\bar{p}(\mathbf{x},t)$.

The density field $\rho(\mathbf{x},t)$, the velocity field $\mathbf{u}(\mathbf{x},t)$, and the combustion progress variable field $c(\mathbf{x},t)$, obtained in the DNS, are filtered out using box (top-hat) filters, see Eq. (12), of different widths Δ, equal to $0.22\delta_L$, $0.44\delta_L$, and $0.88\delta_L$. Moreover, the following Gaussian filter [43,44]

$$G_\Delta(\mathbf{x},\boldsymbol{\xi}) = \frac{1}{\Delta^3}\left(\frac{6}{\pi}\right)^{3/2} \exp\left(-\frac{6|\boldsymbol{\xi}|^2}{\Delta^2}\right) \tag{15}$$

is used with $\Delta = 0.44\delta_L$. When testing Eqs. (13) and (14), the model constants b_D and b_G, respectively, are inserted into these equations, i.e., the following gradient model equations

$$\bar{\tau}(p,\Theta) = \overline{p\Theta} - \bar{p}\bar{\Theta} = \frac{b_D}{12}\Delta^2 \frac{\partial \bar{p}}{\partial x_k}\frac{\partial \bar{\Theta}}{\partial x_k} \tag{16}$$

and

$$\bar{\tau}(\mathbf{u},\nabla p) = \overline{u_i \frac{\partial p}{\partial x_i}} - \bar{u}_i \overline{\frac{\partial p}{\partial x_i}} = \frac{b_G}{12}\Delta^2 \frac{\partial \bar{u}_i}{\partial x_k}\frac{\partial^2 \bar{p}}{\partial x_i \partial x_k}. \tag{17}$$

are assessed. Here, subscripts D and G in b_D and b_G refer to dilatation and gradient, respectively.

In the following, variations of the considered terms within mean flame brush are reported vs. time- and transverse-averaged combustion progress variable by taking advantage of the monotonous increase in $\overline{\langle c\rangle}(x)$ from zero to unity with distance x. Moreover, the terms $\langle \bar{\tau}(p,\Theta)|\bar{c} = \xi\rangle$ and $\langle \bar{\tau}(\mathbf{u},\nabla p)|\bar{c} = \xi\rangle$ conditioned to $|\bar{c}(\mathbf{x},t) - \xi| < \Delta\xi$ and sampled from the entire flame brush over all instances are also reported, with $\Delta\xi = 0.05$.

Results and Discussion

Figure 1 shows variations of subfilter pressure-dilatation term $\bar{\tau}(p,\Theta)$ within mean flame brush, with both time- and transverse-averaged term $\overline{\langle \bar{\tau}(p,\Theta)\rangle}$ and conditioned terms $\langle \bar{\tau}(p,\Theta)|\bar{c} = \xi\rangle$ being presented, see curves plotted in black dots and color lines, respectively. As far as results obtained using the top hat filters are concerned, the following trends are worth noting.

First, magnitudes of both the mean term $\overline{\langle \bar{\tau}(p,\Theta)\rangle}$ and the conditioned terms $\langle \bar{\tau}(p,\Theta)|\bar{c} = \xi\rangle$ are decreased with decreasing the filter width Δ, cf. scales of ordinate axes in Figs. 1a, 1b, and 1d. This observation is associated with the fact that the difference in $\overline{p\Theta}$ and $\bar{p}\bar{\Theta}$ tends to zero as $\Delta \to 0$.

Second, the conditioned terms have the largest magnitude at $\xi = 0.1$ if $\Delta = 0.22\delta_L$, with the term being negative, see curve plotted in violet dashed line in Fig. 1a. If $\Delta = 0.88\delta_L$, the largest magnitude of $\langle \bar{\tau}(p,\Theta)|\bar{c} = \xi\rangle$ is reached at $\xi = 0.7$, with the term being positive, see curve plotted in magenta dotted-double-dashed line in Fig. 1d. At $\Delta = 0.44\delta_L$, magnitudes of the negative $\langle \bar{\tau}(p,\Theta)|c = 0.1\rangle$ and the positive $\langle \bar{\tau}(p,\Theta)|\bar{c} = 0.5\rangle$ are comparable, see Fig. 1b.

Third, as already noted, the conditioned term changes its sign from negative at $\xi = 0.1$ to positive at $\xi = 0.5$ and $\xi = 0.7$, see curves plotted in violet dashed, orange solid, and magenta dotted-doubled-dashed lines, respectively, in Figs. 1a, 1b, or 1d. At $\xi = 0.3$, the term is positive if $\Delta = 0.22\delta_L$, but is negative if $\Delta = 0.44\delta_L$ or $\Delta = 0.88\delta_L$, see curves plotted in blue double-dotted-dashed lines. The observed dependence of the sign of $\langle \bar{\tau}(p,\Theta)|\bar{c} = \xi\rangle$ on the sampling variable ξ can be explained by recalling that the studied flame statistically retains the local structure of the counterpart unperturbed laminar premixed flame [28,29,31,32]. In the latter flame, pressure monotonously decreases from unburned to burned sides, whereas dilatation grows from zero to a peak value reached at $c \approx 0.3$ and decreases with further increasing c. Accordingly, correlation between pressure and dilatation should be negative and positive at $c < c^*$ and $c > c^*$, respectively, with $c^* \approx 0.3$. These simple reasoning explain the opposite signs of $\langle \bar{\tau}(p,\Theta)|c = 0.1\rangle < 0$ and $\langle \bar{\tau}(p,\Theta)|\bar{c} = 0.5\rangle > 0$.

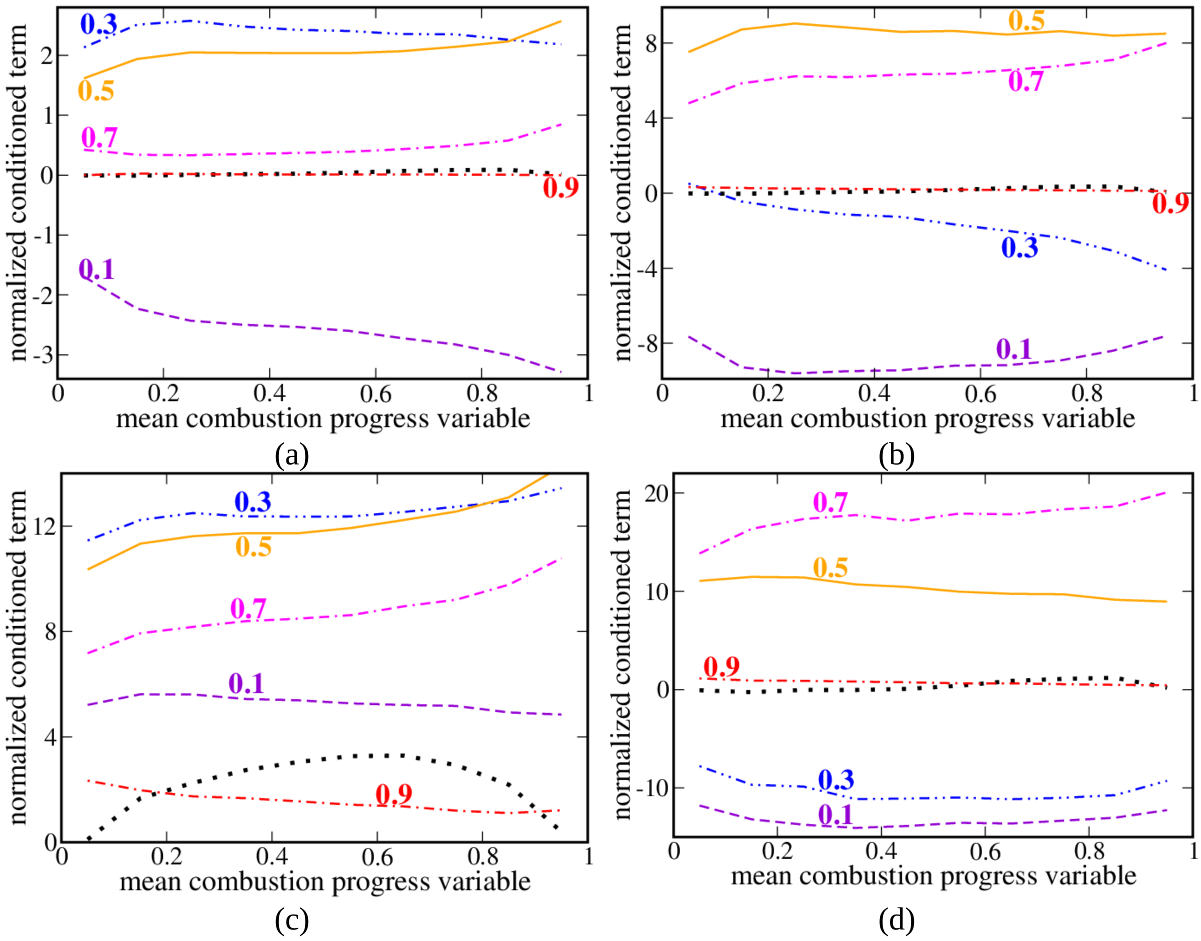

Figure 1. Variations of pressure-dilatation term $\bar{\tau}(p,\Theta)$ within mean flame brush. Black dotted lines show time- and transverse-averaged term $\overline{\langle\bar{\tau}(p,\Theta)\rangle}$. Color lines show conditioned terms $\langle\bar{\tau}(p,\Theta)|\bar{c}=\xi\rangle$, with the values of the conditioning variable ξ being specified near curves. All terms are normalized using $\delta_L/(\rho_u S_L^3)$. (a) Top hat filter, $\Delta = 0.22\delta_L$. (b) Top hat filter, $\Delta = 0.44\delta_L$. (c) Gaussian filter, $\Delta = 0.44\delta_L$. (d) Top hat filter, $\Delta = 0.88\delta_L$.

Fourth, due to the emphasized dependence of the sign of $\langle\bar{\tau}(p,\Theta)|c=\xi\rangle$ on ξ, positive and negative contributions to the mean term $\overline{\langle\bar{\tau}(p,\Theta)\rangle}$ partially counterbalance one another and the mean term magnitudes, see curves plotted in black dots, are much smaller than magnitudes of the conditioned terms sampled at $0.1 \le \xi \le 0.7$. Moreover, these differences in the magnitudes of $\overline{\langle\bar{\tau}(p,\Theta)\rangle}$ and $\langle\bar{\tau}(p,\Theta)|c=\xi\rangle$ are associated with the fact that dilatation is localized to thin zones in a typical premixed turbulent flame and, in particular, in the studied flame [30]. When averaging is performed over a transverse plane, probability of finding such zones is low and the mean terms $\overline{p\Theta}$ and $\bar{p}\bar{\Theta}$ are relatively small. When averaging is performed over volumes characterized by $\bar{c}(\mathbf{x},t) = 0.1$ or 0.5, probability of finding large dilatation is substantial and the magnitude of the conditioned term $\langle\overline{p\Theta}|\bar{c}=\xi\rangle$ or $\langle\bar{p}\bar{\Theta}|\bar{c}=\xi\rangle$ is significantly larger when compared to its mean counterpart.

Dependence of both sign and magnitude of $\langle\bar{\tau}(p,\Theta)|c=\xi\rangle$ on ξ seems to pose a challenge to models of $\bar{\tau}(p,\Theta)$ for LES of premixed turbulent combustion. Even much more serios challenge is revealed by comparing Figs. 1b and 1c, which show that both qualitative behaviour and magnitudes of both mean and conditioned terms are very different for top hat and Gaussian filters, with all other things being equal. These observations are associated with great sensitivity of very small differences $\overline{p\Theta} - \bar{p}\bar{\Theta}$ (see scales of ordinate axes in Figs. 1b or 1c) between very large terms $\overline{p\Theta}$ and $\bar{p}\bar{\Theta}$, see Fig. 2a, to small variations in numerics. Note that $\overline{\langle \bar{p}\bar{\Theta}\rangle}\left(\overline{\langle c\rangle}\right)$- and $\overline{\langle p\Theta\rangle}\left(\overline{\langle c\rangle}\right)$-curves are indistinguishable in Fig. 2a, as well as curves obtained using top hat and Gaussian filters (cf. black and red curves) or different filter widths (not shown for brevity). Since independence of results on the choice of filter shape is a cornerstone hypothesis of LES, comparison of Figs. 1b and 1c calls into question the utility of adopting the terms $\overline{p\Theta}$ and $\bar{p}\bar{\Theta}$ in LES of premixed turbulent flames.

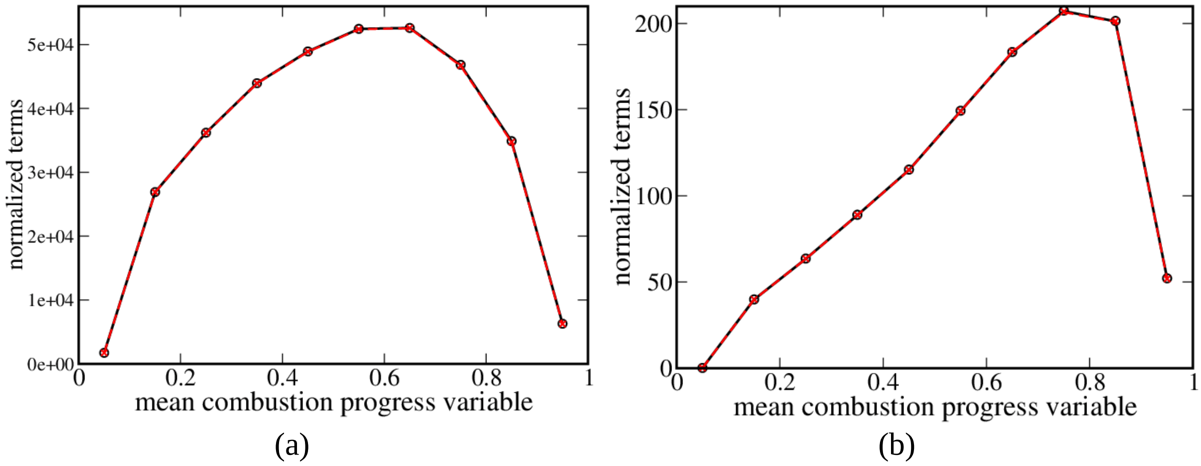

Figure 2. Variations of time- and transverse-averaged terms (a) $\overline{\langle \bar{p}\bar{\Theta}\rangle}$ (lines) and $\overline{\langle p\Theta\rangle}$ (symbols) or (b) $-\overline{\langle \bar{\mathbf{u}}\cdot\nabla\bar{p}\rangle}$ (lines) and $-\overline{\langle \mathbf{u}\cdot\nabla p\rangle}$ (symbols) and within mean flame brush. $\Delta = 0.44\delta_L$. Black and red lines/symbols show results obtained using top hat and Gaussian filters, respectively. All terms are normalized using $\delta_L/(\rho_u S_L^3)$.

Comparison of scales of ordinate axes in Figs. 2b and 3 shows that $\left|\overline{\langle \bar{\mathbf{u}}\cdot\nabla\bar{p}\rangle}\right|$ and $\left|\overline{\langle \mathbf{u}\cdot\nabla p\rangle}\right|$ are also significantly larger than $\left|\overline{\langle \bar{\mathbf{u}}\cdot\nabla\bar{p}\rangle} - \overline{\langle \mathbf{u}\cdot\nabla p\rangle}\right|$. However, the difference in magnitudes of $\left|\overline{\langle \bar{\mathbf{u}}\cdot\nabla\bar{p}\rangle}\right|$ or $\left|\overline{\langle \mathbf{u}\cdot\nabla p\rangle}\right|$ and $\left|\overline{\langle \bar{\mathbf{u}}\cdot\nabla\bar{p}\rangle} - \overline{\langle \mathbf{u}\cdot\nabla p\rangle}\right|$ is much smaller than the counterpart difference for the pressure-dilatation terms, e.g., scales of ordinates axes in Figs. 1a and 3a, 1b and 3b, or 1d and 3d are comparable, whereas scale of ordinate axis in Fig. 2a is much larger when compared to Fig. 2b. Therefore, sensitivity of $\bar{\tau}(\mathbf{u},\nabla p)$ to numerics is significantly less pronounced and similar results are obtained using top hat and Gaussian filters with $\Delta = 0.44\delta_L$, cf. Figs. 3b and 3c.

With the exception of this very important difference between $\bar{\tau}(p,\Theta))$ and $\bar{\tau}(\mathbf{u},\nabla p)$, other trends observed in Figs. 1 and 3 are similar. Specifically, first, magnitudes of both the mean term $\overline{\langle \bar{\tau}(\mathbf{u},\nabla p)\rangle}$ and the conditioned terms $\langle \bar{\tau}(\mathbf{u},\nabla p)|\bar{c}=\xi\rangle$ are decreased with decreasing the filter width Δ, cf. scales of ordinate axes in Figs. 3a, 3b, and 3d. Second, magnitude of the mean term $\overline{\langle \bar{\tau}(\mathbf{u},\nabla p)\rangle}$ is much smaller than magnitudes of the conditioned terms $\langle \bar{\tau}(\mathbf{u},\nabla p)|\bar{c}=\xi\rangle$ sampled at $0.1 \le \xi \le 0.7$ Third, both magnitude and sign of $\langle \bar{\tau}(\mathbf{u},\nabla p)|\bar{c}=\xi\rangle$ vary significantly with the sampling variable ξ, e.g., this term is negative at $\xi = 0.1$ or 0.3, see curves plotted in violet dashed or blue double-dotted-dashed lines in Fig. 3 and note that this curves show $\langle -\bar{\tau}(\mathbf{u},\nabla p)|\bar{c}=\xi\rangle$, because the rhs of Eq. (2) involves $-\bar{\tau}(\mathbf{u},\nabla p)$. On the contrary, $\langle \bar{\tau}(\mathbf{u},\nabla p)|\bar{c}=0.7\rangle > 0$, see curves plotted in magenta dotted-double-dashed lines.

Results of assessing gradient models of both $\bar{\tau}(p,\Theta)$ and $\bar{\tau}(\mathbf{u},\nabla p)$ are plotted in Fig. 4 in red and black lines, respectively. With the exception of $\overline{\langle \bar{\tau}(p,\Theta)\rangle}$ yielded by the Gaussian filter, the DNS data (solid lines) are reasonably well predicted by the gradient models without any tuning, i.e., by Eqs. (16)-(17) with $b_D = b_G = 1$ (dashed lines).

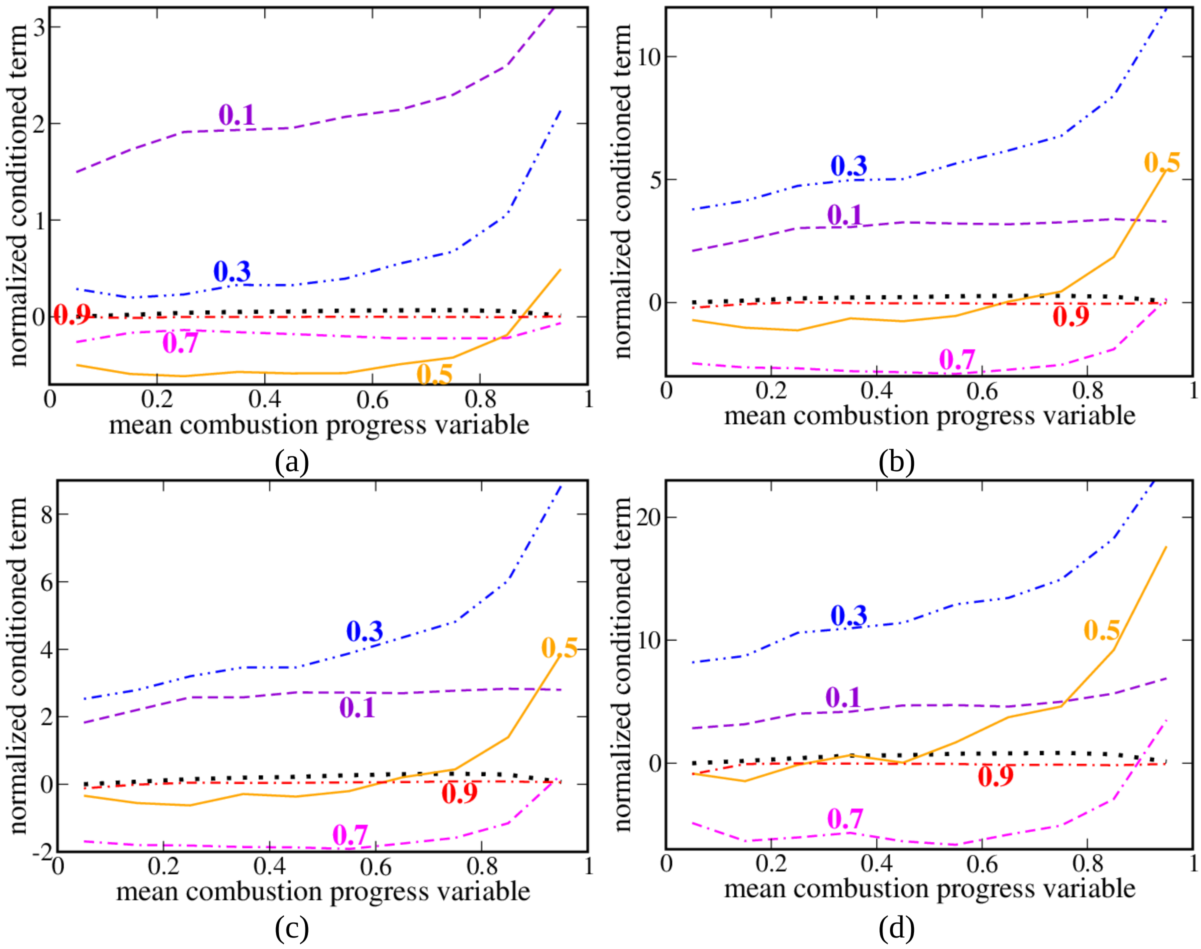

Figure 3. Variations of velocity-pressure-gradient term $\bar{\tau}(\mathbf{u}, \nabla p)$ within mean flame brush. Black dotted lines show time- and transverse-averaged term $\overline{\langle -\bar{\tau}(\mathbf{u}, \nabla p) \rangle}$. Color lines show conditioned terms $\langle -\bar{\tau}(\mathbf{u}, \nabla p) | \bar{c} = \xi \rangle$, with the values of the conditioning variable ξ being specified near curves. All terms are normalized using $\delta_L/(\rho_u S_L^3)$. (a) Top hat filter, $\Delta = 0.22\delta_L$. (b) Top hat filter, $\Delta = 0.44\delta_L$. (c) Gaussian filter, $\Delta = 0.44\delta_L$. (d) Top hat filter, $\Delta = 0.88\delta_L$.

Nevertheless, difference between the DNS and model results increases with increasing the filter width Δ, cf. Figs. 4a and 4d. Predictions can be significantly improved by tuning the constants b_D and b_G in Eqs. (16) and (17), respectively, cf. curves plotted in solid and dotted lines. It is remarkable that the curve shapes are well predicted in all cases with the exception of $\bar{\tau}(p, \Theta)$ computed by adopting the Gaussian filter. Results obtained by tuning b_D in that case are not shown in Fig. 4c, because the use of very large values of model constants does not seem to be basically justified.

The tuned values of b_D and b_G reported in Table 1, show a gradual increase with Δ. Nevertheless, the tuned values remain of unity order and this fact implies that gradient models are promising even for the pressure-containing terms. However, it is worth noting that the largest filter width used in the present work is on the order of laminar flame thickness. Such a limitation is typical for *a priori* analysis of DNS data obtained from three-dimensional complex chemistry turbulent flames, because a ratio of computational width to δ_L is still rather moderate in such simulations reviewed elsewhere [45]. Accordingly, substantially larger values of b_G may be expected for larger Δ/δ_L. Under such conditions, dynamic-modelling approach pioneered by Germano et al. [46] could be used to determine b_G. In any case, close agreement between curves plotted in solid and dotted lines in Fig. 4 lends support to gradient models.

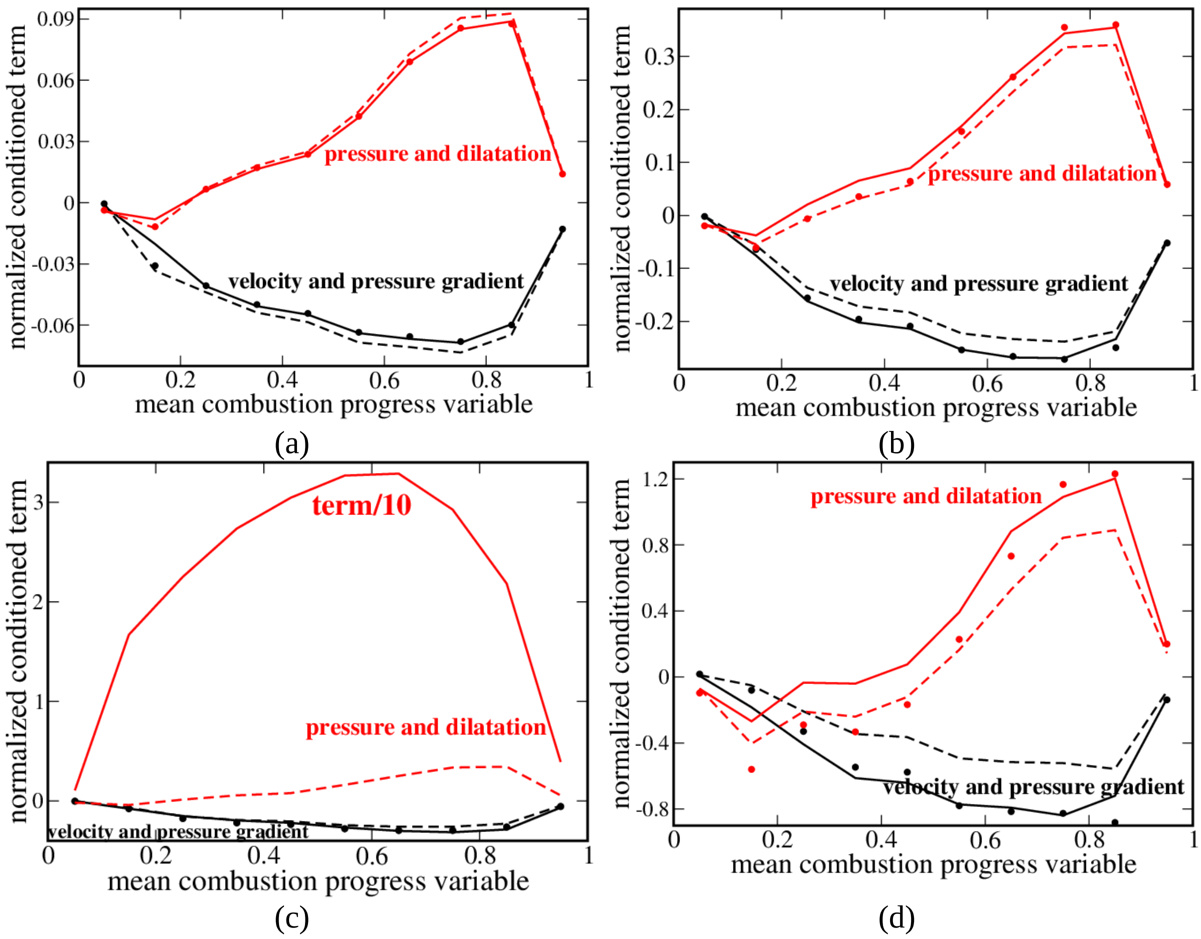

Figure 4. Assessment of gradient models for subfilter pressure-dilatation term $\bar{\tau}(p,\Theta)$ (red lines) and subfilter velocity-pressure-gradient term $\bar{\tau}(\mathbf{u},\nabla p)$ (black lines). Solid lines show time- and transverse-averaged terms $\overline{\langle\bar{\tau}(p,\Theta)\rangle}$ and $\overline{\langle\bar{\tau}(\mathbf{u},\nabla p)\rangle}$. Dashed lines show results yielded straightforwardly by gradient models, see Eqs. (16) and (17) with the constants $b_D = b_G = 1$. Dotted lines show results yielded by gradient models with tuned values of the constants b_G and b_D, reported in Table 1. All terms are normalized using $\delta_L/(\rho_u S_L^3)$. (a) Top hat filter, $\Delta = 0.22\delta_L$. (b) Top hat filter, $\Delta = 0.44\delta_L$. (c) Gaussian filter, $\Delta = 0.44\delta_L$. (d) Top hat filter, $\Delta = 0.88\delta_L$.

Table 1. Tuned values of model constants.

Filter	b_D in Eq. (16)	b_G in Eq. (17)
Top hat, $\Delta = 0.22\delta_L$	0.94	0.93
Top hat, $\Delta = 0.44\delta_L$	1.12	1.14
Gaussian, $\Delta = 0.44\delta_L$	-	1.15
Top hat, $\Delta = 0.88\delta_L$	1.39	1.59

Recently, Wang et al. [12] supported the following equation:

$$\overline{u_i \frac{\partial p}{\partial x_i}} - \tilde{u}_i \frac{\partial \bar{p}}{\partial x_i} = C_p \Delta^2 \frac{\partial \tilde{u}_i}{\partial x_k} \frac{\partial^2 \bar{p}}{\partial x_i \partial x_k} \tag{18}$$

in their a priory analysis of DNS data obtained from a premixed swirling flame. However, to get good agreement between Eq. (18) and those DNS data, Wang et al. [12, Fig. 3] were forced to significantly increase C_p when compared to 1/12. On the face of it, these recent results are inconsistent with the present analysis. However, this is not so, because the lhs of Eq. (18) differs from $\bar{\tau}(\mathbf{u}, \nabla p)$ analysed by us. Indeed,

$$\overline{u_i \frac{\partial p}{\partial x_i}} - \tilde{u}_i \frac{\partial \bar{p}}{\partial x_i} = \overline{u_i \frac{\partial p}{\partial x_i}} - \bar{u}_i \frac{\partial \bar{p}}{\partial x_i} + (\bar{u}_i - \tilde{u}_i) \frac{\partial \bar{p}}{\partial x_i} = \bar{\tau}\left(u_i, \frac{\partial p}{\partial x_i}\right) + (\bar{u}_i - \tilde{u}_i) \frac{\partial \bar{p}}{\partial x_i}, \qquad (19)$$

i.e., the closure relation assessed by Wang et al. [12] differs from the gradient model explored by us, see Eq. (17). Moreover, the right hand sides of Eqs. (17) and (19) involve $\partial \bar{u}_i / \partial x_k$ and $\partial \tilde{u}_i / \partial x_k$, respectively.

Conclusions

Pressure-dilatation and velocity-pressure-gradient terms in transport equations for subfilter turbulent kinetic energy were *a priori* explored by analyzing three-dimensional DNS data obtained by Dave et al. [13,14] from a moderately lean complex-chemistry hydrogen-air flame propagating in moderately intense, small-scale turbulence in a box. The terms were computed by filtering out the DNS fields of velocity, density, pressure, and fuel mass fraction and adopting Gaussian or top hat filters of different widths, which were smaller or comparable with laminar flame thickness.

In addition, gradient models of the second order generalized central moments (joint cumulants), which were mainly applied to subfiter turbulent stresses and scalar fluxes in various flows, were further extended to close the explored pressure-containing terms.

The reported numerical results give priority to using the velocity-pressure-gradient term when compared to the pressure-dilatation term, because the former term is weakly sensitive to filter shape, whereas the latter term evaluated adopting the Gaussian filter is significantly larger than the same term yielded by the top-hat filter of the same width. The latter result is associated with great sensitivity of a small difference in two very larger quantities to numerics.

Moreover, spatial variations of time- and transverse averaged velocity-pressure-gradient term within mean flame brush were shown to be well predicted by the newly introduced gradient model in all studied cases (different filter shapes or widths). While the sole model constant tuned to get the best prediction increases gradually with filter width, the constant remains of unity order in all cases. These results encourage further assessment of gradient models as a promising tool for LES research into premixed turbulent combustion.

References

[1] Karlovitz, B., Denniston, D.W., Wells, F.E., "Investigation of turbulent flames", J. Chem. Phys. 19: 541-547 (1951).

[2] Scurlock, A.C., Grover, J.H., "Propagation of turbulent flames", *Proc. Combust. Inst*. 4: 645-658 (1953).

[3] Lipatnikov, A.N., Chomiak, J., "Effects of premixed flames on turbulence and turbulent scalar transport", *Prog. Energy Combust. Sci*. 36: 1-102 (2010).

[4] Sabelnikov, V.A., Lipatnikov, A.N., "Recent advances in understanding of thermal expansion effects in premixed turbulent flames", *Annu. Rev. Fluid Mech*. 49: 91-117 (2017).

[5] Steinberg, A.M., Hamlington, P.E., Zhao, X., "Structure and dynamics of highly turbulent premixed combustion", *Prog. Energy Combust. Sci*. 85: 100900 (2021).

[6] Chakraborty, N., "Influence of thermal expansion on fluid dynamics of turbulent premixed combustion and its modelling implications", *Flow Turbul. Combust*. 106: 753-848 (2021).

[7] Zhang, S., Rutland, C.J., "Premixed flame effects on turbulence and pressure related terms", *Combust. Flame* 102: 447-461 (1995).
[8] Nishiki, S., Hasegawa, T., Borghi, R., Himeno, R., "Modeling of flame-generated turbulence based on direct numerical simulation databases", *Proc. Combust. Inst*. 29: 2017-2022 (2002).
[9] O'Brien, J., Towery, C.A.Z., Hamlington, P.E., Ihme, M., Poludnenko, A.Y., Urzay J., "The cross-scale physical-space transfer of kinetic energy in turbulent premixed flames", *Proc. Combust. Inst.* 36: 1967-1975 (2017).
[10] Lee, J., MacArt, J.F., Mueller, M.E., "Heat release effects on the Reynolds stress budget in turbulent premixed jet flames at low and high Karlovitz numbers", *Combust. Flame* 216: 1-8 (2020).
[11] Su, Y., Lu, Z., Yang, Y., "Suppression of the turbulent kinetic energy and enhancement of the flame-normal Reynolds stress in premixed jet flames at small Lewis numbers", *Combust. Flame* 246: 112461 (2022).
[12] Wang, Y., Luo, K., Xiao, H., Jin, T., Xing, J., Fan, J., "A novel subgrid-scale stress model considering the influence of combustion on turbulence: *A priori* and *a posteriori* assessment", *Phys. Fluids* 36: 085161 (2024).
[13] Dave, H.L., Mohan, A., Chaudhuri, S., "Genesis and evolution of premixed flames in turbulence", *Combust. Flame* 196: 386-399 (2018).
[14] Dave, H.L., Chaudhuri, S., "Evolution of local flame displacement speeds in turbulence", *J. Fluid Mech*. 884: A46 (2020).
[15] Stratonovich, R.L., *Topics in the Theory of Random Noise*, vol. 1, Gordon and Breach, NY, 1963.
[16] Germano, M., "Turbulence: the filtering approach", *J. Fluid Mech*. 238: 325-336 (1992).
[17] Leonard, A., "Energy cascade in large-eddy simulations of turbulent fluid flows", *Adv. Geophys*. 18: 237-248 (1974).
[18] Clark, R.A., Ferziger, J.H., Reynolds, W.C., "Evaluation of subgrid-scale models using an accurately simulated turbulent flow", *J. Fluid Mech*. 91: 1-16 (1979).
[19] Tullis, S., Cant, R.S., "Scalar transport modeling in large eddy simulation of turbulent premixed flames", *Proc. Combust. Inst*. 29: 2097-2105 (2002).
[20] Vreman, A.W., van Oijen, J.A., de Goey, L.P.H., Bastiaans, R.J.M., "Subgrid scale modeling in large-eddy simulation of turbulent combustion using premixed flamelet chemistry", *Flow Turbul. Combust*. 82: 511-535 (2009).
[21] Galeazzo, F.C.C., Savard, B., Wang, H., Hawkes, E.R., Chen, J.H., Filho, G.C.K., "Performance assessment of flamelet models in flame-resolved LES of a high Karlovitz methane/air stratified premixed jet flame", *Proc. Combust. Inst*. 37: 2545-2553 (2019).
[22] Keil, F.B., Klein, M., Chakraborty, N., "Sub-grid reaction progress variable variance closure in turbulent premixed flames", *Flow Turbul. Combust*. 106: 1195-1212 (2020).
[23] Nikolaou, Z., Domingo, P., Vervisch, L., "Revisiting the modelling framework for the unresolved scalar variance", *J. Fluid Mech*. 983: A47 (2024).
[24] Liu, S., Meneveau, C., Katz, J., "On the properties of similarity subgrid-scale models as deduced from measurements in a turbulent jet", *J. Fluid Mech*. 275: 83-119 (1994).
[25] Cimarelli, A., Abba, A., Germano, M., "General formalism for a reduced description and modelling of momentum and energy transfer in turbulence", *J. Fluid Mech*. 866: 865-896 (2019).
[26] Berselli, L.C., Iliescu, T., Layton, W.J., *Mathematics of Large Eddy Simulation of Turbulent Flows*, Springer, 2006.
[27] Bardina, J., Ferziger, J., Reynolds, W., "Improved subgrid scale models for large eddy simulation", *AIAA Paper* 801357, 1980.

[28] Lipatnikov, A.N., Sabelnikov, V.A., "An extended flamelet-based presumed probability density function for predicting mean concentrations of various species in premixed turbulent flames", *Int. J. Hydrogen Energy* 45: 31162-31178 (2020).
[29] Lipatnikov, A.N., Sabelnikov, V.A., "Evaluation of mean species mass fractions in premixed turbulent flames: A DNS study", *Proc. Combust. Inst*. 38: 6413-6420 (2021).
[30] Sabelnikov, V.A., Lipatnikov, A.N., Nishiki, S., Dave, H.L., Hernández-Pérez, F.E., Song, W., Im, H.G., "Dissipation and dilatation rates in premixed turbulent flames", *Phys. Fluids* 33: 035112 (2021).
[31] Lipatnikov, A.N., Sabelnikov, V.A., "Flame folding and conditioned concentration profiles in moderately intense turbulence", *Phys. Fluids* 34: 065119 (2022).
[32] Lipatnikov, A.N., Sabelnikov, V.A., "Influence of small-scale turbulence on internal flamelet structure", *Phys. Fluids* 35: 055128 (2023).
[33] Lipatnikov, A.N. "A priori test of perfectly stirred reactor approach to evaluating mean fuel consumption and heat release rates in highly turbulent premixed flames", *Int. J. Engine Res*. 24: 4034-4043 (2023).
[34] Lipatnikov, A.N., Sabelnikov, V.A., Nikitin, N.V., "Opposite effects of flame-generated potential and solenoidal velocity fluctuations on flame surface area in moderately intense turbulence", *Proc. Combust. Inst*. 40: 105238 (2024).
[35] Lipatnikov, A.N., "A priori assessment of a simple approach to evaluating burning rate in large eddy simulations of premixed turbulent combustion", *Phys. Fluids* 36: (2024).
[36] Babkovskaia, N., Haugen, N.E.L., Brandenburg, A., "A high-order public domain code for direct numerical simulations of turbulent combustion", *J. Comput. Phys*. 230: 1-12 (2011).
[37] Li, J., Zhao, Z., Kazakov, A., Dryer, F.L., "An updated comprehensive kinetic model of hydrogen combustion", *Int. J. Chem. Kinetics* 36: 566-575 (2004).
[38] Poinsot, T.J., Lele, S.K., "Boundary conditions for direct simulations of compressible viscous flows", *J. Comput. Phys*. 101: 104-129 (1992).
[39] Lipatnikov, A.N., Chomiak, J., "Molecular transport effects on turbulent flame propagation and structure", *Prog. Energy Combust. Sci*. 31: 1-73 (2005).
[40] Hochgreb, S., "How fast can we burn, 2.0?" *Proc. Combust. Inst*. 29: 2077-2105 (2023).
[41] Pitsch, H., "The transition to sustainable combustion: Hydrogen- and carbon-based future fuels and methods for dealing with their challenges", *Proc. Combust. Inst*. 40: 105638 (2024).
[42] Lipatnikov, A.N., Sabelnikov, "Karlovitz numbers and premixed turbulent combustion regimes for complex-chemistry flames", *Energies* 15: 5840 (2022).
[43] Piomelli, U., "Large-eddy simulation: achievements and challenges", *Prog. Aerospace Sci*. 35: 335-362 (1999).
[44] Lees, A., Aluie, H., "Baropycnal work: A mechanism for energy transfer across scales", *Fluids* 4: 92 (2019).
[45] Domingo, P., Vervisch, L., "Recent developments in DNS of turbulent combustion", *Proc. Combust. Inst*. 39: 2055-2076 (2023).
[46] Germano, M., Piomelli, U., Moin, P., Cabot, W.H., "A dynamic subgrid-scale eddy viscosity model", *Phys. Fluids A* 3: 1760-1765 (1991).